LANGMUIR



Interface Components: Nanoparticles, Colloids, Emulsions, Surfactants, Proteins, Polymers

# Label-free Exosomal Detection Based on a Low-cost Plasmonic Biosensor Array Integrated with Microfluidics

Xiaoqing Lv, zhaoxin geng, Yue Su, Zhiyuan Fan, Shicai Wang, Weihao Fang, and Hongda Chen

*Langmuir*, **Just Accepted Manuscript** • DOI: 10.1021/acs.langmuir.9b01237 • Publication Date (Web): 03 Jul 2019



is published by the American Chemical Society. 1155 Sixteenth Street N.W., Washington, DC 20036

# Label-free Exosome Detection Based on a Low-cost Plasmonic Biosensor Array Integrated with Microfluidics

Xiaoqing Lv[1], Zhaoxin Geng[1,2]*, Yue Su[1,3], Zhiyuan Fan[1,3], Shicai Wang[1,4], Weihao Fang[1,3] and Hongda Chen[1]

1 State Key Laboratory of Integrated Opoelectronics, Institute of Semiconductors, Chinese Academy of Science, Beijing 100083, China

2 School of Information Engineering, Minzu University of China, Beijing 100081, China

3 College of Materials Science and Opto-Electronic Technology, University of Chinese Academy of Sciences, Beijing 100049, China

4 State Key Laboratory of Crystal Materials, Shandong University, Jinan 250022, China

## Abstract

LSPR-based plasmonic biosensors have been interesting candidates for the design of portable optical biosensor platforms owing to their integration, miniaturization, multi-parameter, real-time, and label-free detection characteristics. Plasmonic biosensor arrays that have been combined with microfluidics have been developed herein to label-free detect exosomes. Gold nano-ellipsoid arrays were fabricated with low-cost anodic aluminum oxide (AAO) thin films that acts as shadow-masks for evaporation of Au. The nano-ellipsoid arrays were integrated with microfluidic chip to achieve multi-parameter detection. The anti-CD63 antibody that is specific to the exosome transmembrane protein CD63is modified on the surface of the nano-ellipsoids. Exosomes were injected into the biosensor platform at different concentrations and detected successfully. The detection limit was 1 ng/mL. The proposed plasmonic biosensor array can be universally applicable for the detection of other biomarkers by simply changing the antibody on the surface of the Au nano-ellipsoids. Moreover, this biosensor platform is envisaged to be potentially useful in the development of low-cost plasmonic-based biosensors for biomarker detection and for the investigation of exosomes for non-invasive disease diagnoses.

## Introduction

Exosomes (ranging in size from 40 to 100 nm) are cell-derived extracellular vesicles types, and are present in biological fluids, including blood, urine, cerebrospinal fluid, ascites, and in other moieties, and constitute novel biomarkers for the monitoring and prediction cancer diseases.[1–4] Despite their potential for clinical use, the lack of a sensitive detection method for exosomes poses a barrier to clinical translation. Traditional methods to isolate exosomes, such as ultracentrifugation, density gradient centrifugation, are time-consuming, and are associated with increased costs, and require for expensive instruments that ultimately limit their clinical applications.[5] There are many novel approaches based on microfluidic technology that are used to isolate and detect exosomes from liquid samples, such as size-based exosome isolation [6], high-throughput and high-specificity immunoisolation,[7,8] electrochemical detection using quantum dots,[9] graphene oxide/ polydopamine (GO/PDA) nano-interface isolation,[10] alternating current electrohydrodynamically induced nanoshearing detection,[11] and Anion-exchange-based detection.[12] Microfluidic technology could functionalize the biosensor quantitatively, reduce

consumption, reduce reaction time during the experiment,[13] and detect exosomes in low-sample volumes within a few hours.[14]

Nanoplasmonic-based biosensors, which are of great interest in various application in view of their numerous promising features, such as high sensitivity, real-time, and label-free detection,[15] N have been utilized as an effective platform to quantitatively detect tumor biomarkers, deoxyribonucleic acid (DNA), and other biological proteins and molecules.[16–21] A biosensor based on localized surface plasmon resonance (LSPR) was integrated with a microfluidic chip to form a LSPR-based microfluidic platform. It has been established that LSPR-based detection methods are excellent candidates for the sensitive, specific, and portable analysis of biomarkers. For example, Im et al. developed an nPLEX assay where a periodic nanohole array device was used to analyze ascite samples from ovarian cancer patients.[22] Thakur et al. developed a LSPR-based biosensor with self-assembled gold nanoislands to detect and distinguish exosomes from different cell lines.[21] Bonyár et al. investigated the performance of gold nanoislands for LSPR application.[23] Although the sensitivities of these methods are much better than those of traditional methods, their applications are not widespread owing to their high-costs. Moreover, the fabrication procedure of these methods is complex and requires professional training. There has been increasing interest in the development of new biosensor platforms with a) lower costs, b) that can be easily fabricated and c) have better sensitivity responses suitable that are adequate for the requirements of the rapidly expanding exosome research and applications.

To improve the detection of nanoscale biological analytes, nanostructures fabrication is essential during fabrication of the LSPR-based biosensor.[24] The regular LSPR nanostructures, such as nanoholes,[25] nanopillars,[26] and nanodisks,[27] nanorods,[28] and nanoantennas,[29] are fabricated by electron beam lithographic or mask-assist techniques, and require complex synthetic processes and entail increased costs. In prior studies, the random LSPR nanostructures were investigated in depth and their costs were reduced by sacrificeing the sensitivity of the biosensor.[21,23] It is still challenging to obtain ordered arrays on substrates in a facile manner.[30] To solve the problems mentioned above, low-cost methods used to fabricate metal nanostructures with large areas and uniformities are necessary for the application of LSPR-based biosensors. Anodic aluminum oxide (AAO) has been extensively used as a template to fabricate nanostructure because the aspect ratio, diameter, and length of the core in AAO can be easily controlled by voltage, temperature, electrolytes and anodization time. By placing the AAO templates onto different substrates, nanodot arrays can be obtained through vapor deposition.[30–34]

Herein, a simple, easy to operate, low-cost fabrication process, and sensitive LSPR-based biosensor that is integrated with a microfluidic chip to functionalize the sensor substrate quantitatively, is presented to detect the exosomes. Highly ordered nano-ellipsoid arrays were fabricated on the substrate based on the use of the AAO thin film that acted as a shadow-mask for evaporating Au. The nano-ellipsoid arrays were functionalized with an anti-CD63 antibody and with an adequate affinity for the detection of exosomes in buffer solutions. With target-specific exosome binding, the biosensor displays extinction spectral shifts to different refractive indices.

The performance of the LSPR-based nano-biosensor was demonstrated using the detection of different refractive index solutions and exosomes in buffer. Atomic force microscopy (AFM), transmission electron microscopy (TEM) and scanning electron microscopy (SEM) images were used to demonstrate the functionalities of the nano-ellipsoid arrays and the captured exosomes.

## Experimental details

### Materials and regents

Ethanol, NaCl, glycol and glycerol were purchased from Sinopharm Chemical Reagent Beijing, Co. Ltd. AAO filter membranes (diameter: 20 mm, thickness: 100 nm, pore size: 90 nm, and a center-to-center hole distance: 125 nm) were purchased from Shenzhen TopMembranes Inc. Deionized water was purchased from Solarbio Beijng, Co. Ltd. Polydimethylsiloxane(PDMS) was obtained from Dow Corning. Thiolated alkane 10-carboxy-1-decanethiol (HS-(CH2)10-COOH), 1-ethyl-3-(3-dimethylamino-propyl) carbodiimide-HCl (EDC), sulfo-nhydroxysuccinimide (S-NHS) and bovine serum albumin (BSA) were purchased from Sigma–Aldrich. Phosphate buffer solution (phosphate buffer solution (PBS): 0.01 M, pH: 7.4, Hyclone) was purchased from Thermo Fisher. Anti-CD63 antibody (1 mg/mL) was purchased from Abcam. The lyophilized exosome standards which was isolated from COLO1 cell culture supernatants with an ultracentrifugation method were purchased from HansaBioMed Life Sciences Ltd.

### Nano-epllisoids fabrication

Fig. 1 shows the illustration of fabrication processes of the gold nano-epllisoids based on the AAO thin film. The nanostructures were produced on a substrate using electron beam evaporation and thermal anneal. First, the substrate (quartz and silicon) wafer (thickness: 1 mm, width: 20 mm, length: 20 mm) were cleaned by successive immersion in solutions of acetone, ethanol, and deionized water (5 min in each solvent), followed by drying in the presence of clean nitrogen flow to enhance the adhesion of the AAO film to the substrate. The substrates were then dipped in a piranha solution (30% $H_2O_2$–70% $H_2SO_4$) for at least 1 h to eliminate the organic residue, rinsed with water, and dried with nitrogen gun. The AAO template was transferred to acetone to thoroughly dissolve the polymethyl methacrylate (PMMA), and template was then suspended in acetone. The substrate wafer was soaked in the acetone. The AAO film was then pulled from acetone and was adhered to the substrate (Fig. 1a). A nine-hole Al shadow-mask was then placed on the substrate after transfer (Fig. 1b). A 30 nm Au film was deposited using electron beam evaporation at the rate of 0.2 Å/s (Fig. 1c). The AAO film was peeled off from the substrate by using Kapoton tape. The gold nanoparticle arrays were then annealed at a high temperature to cause agglomeration into arrays of elliptical nanoparticles by surface tension force (Fig. 1d). Fabrication of the PDMS microchannel has been described in detail in a previous study.[16] The basic steps included the silicon mould fabrication (Fig. 1e), the pouring of PDMS (Fig. 1f), and

the peeling of PDMS (Fig. 1g). Finally, oxygen plasma treatment using a plasma cleaner (PDC–32G, Harrick Scientific Products, Inc.) was used to bond the PDMS microchannel to the sensor substrate irreversiblythat resulted in the complete LSPR-based biosensor (Fig. 1h).

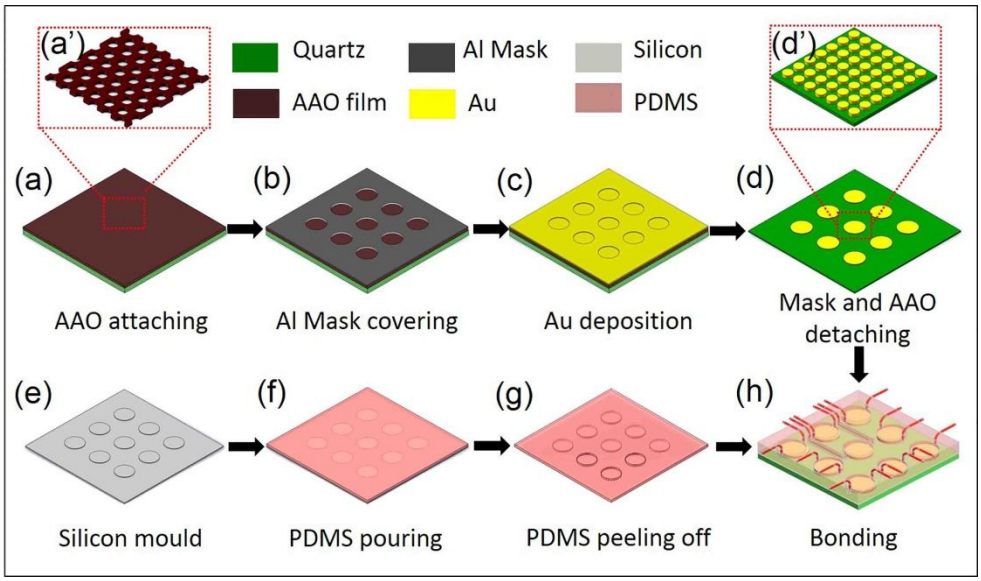


Figure 1. Fabrication process of the localized surface plasmon resonance (LSPR)-based LSPR-based biosensor. (a) Anodic aluminum oxide (AAO) film was transferred onto the quartz substrate. (b) Al mask with multi-hole was covered on the AAO film. (a') is the partially enlarged view of (a). (c) Gold was then deposited on the substrate. (d) The Al mask and the AAO film were peeled off, and the substrate of LSPR-based biosensor was completely fabricated. (d') Partial enlarged view of (d). (e) Silicon mould was fabricated by photolithography and an etching process. (f) Polydimethylsiloxane (PDMS) mixture was poured into the silicon mould and was cured using heating. (g) PDMS was peeled off from the silicon mould. (h) Inlet and outlet holes were punched and the chip was bonded to the substrate of the biosensor.

## LSPR-based biosensor functionalization

To achieve label-free detection of exosomes, anti-CD63 antibody was used to functionalize the biosensor. A schematic of the exosome detection procedure using the LSPR-based biosensor is shown in Fig. 2. The LSPR-based biosensor was functionalized with thiolated alkane 10-carboxy-1-decanethiol (HS-$(CH_2)_{10}$-COOH) through ligand exchange, and was subsequently activated using EDC/NHS coupling chemistry, as noted in a previous study.[35] The sensor was then functionalized with the CD63 antibody. Specifically, a stock solution of HS-$(CH_2)_{10}$-COOH was diluted to 1 mM in 100% ethanol, and was loaded into the biosensor at room temperature for 1 h. The stronger affinity of the thiol anchor group with the gold nano-ellipsoids surface can serve as a linker to the antibody (Fig. 2a, b). A mixture comprising 0.4 M EDC and 0.1 M NHS at a 1:1 volume ratio in a water solution was then loaded into the biosensor and activated the carboxyl moiety on the gold nanoparticles. After surface activation, the CD63 antibody (concentration of 10 μg/mL) was loaded into the biosensor (Fig. 2c). The functionalized LSPR-based biosensor was stored at 4°C in a refrigerator before use.

Exosomes capture and detection

The concentration of exosomes in the buffer solution was determined by the commercial protocol. Lyophilized exosomes were dissolved in ultrapure water and were diluted with a PBS solution to a concentration of 10 μg/m. The samples were then prepared by spiking designated volumes of exosomes in PBS (1 mM, pH 7.0) to obtain the desired sample dilutions (1:10 to $1:1\times10^5$). All the samples were stored at -80°C until further use. All the exosomes samples were loaded into the previously functionalized LSPR-based biosensors for detection. When the testing process was executed, a certain volume of exosomes samples was injected into the biosensor to capture the exosomes (Fig. 2d). The transmission spectra of the sample were detected on the LSPR platform and the spectra was read by the spectrometer and were displayed on the computer (Fig. 2e and Fig. S1).

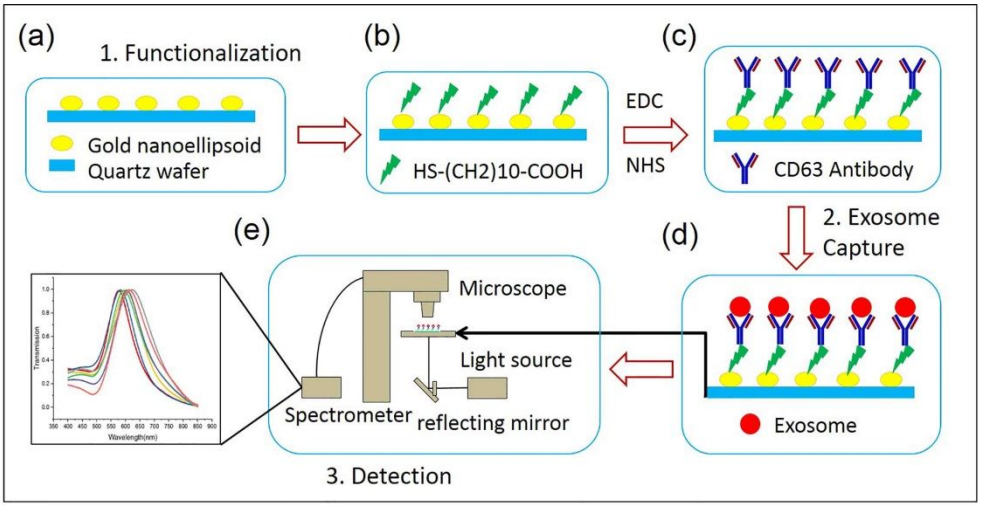


Figure 2. Schematic of the LSPR-based biosensor. (a) Fabrication of gold nano-ellipsoid arrays on the quartz substrate. (b) HS-(CH2)10-COOH was assembled onto the gold nano-ellipsoids with the Au-S bond. (c)The sensor was functionalized with human anti-CD63 antibody after it was activated with EDC and NHS. (d) Exosomes were injected into the microchannel and captured on the sensor substrate. (e) Transmitted spectra were detected using the LSPR detecting platform.

FDTD simulations

The limit of detection of LSPR-based biosensor measurement was theoretically estimated by performing a finite difference time domain (FDTD) simulation that predicted the scattering efficiency on the gold nano-ellipsoids. We have determined the nano-ellipsoids characteristics (radius and height) that led to the best theoretical LSPR response. Additionally, we conducted simulations with different substances and different refractive indices (air, water, 1 M glucose, ethanol, and NaCl solution (5%, 10%, 15%, 20%, and 25%)), and the outcomes were referred to the experimental results.

LSPR-based biosensorCharacterization

The morphologies of the gold nano-ellipsoid arrays were characterized by AFM, TEM, and SEM. The exosome standard was fixed with 4% paraformaldehyde, and was then transferred onto an EM grid and absorbed for 15 min. The exosomes were then treated with contrast staining with uranyl oxalate and methylcellulose mixture. Finally, the exosomes were imaged with a TEM after air drying. The exosome standard was fixed with Karnovsky's fixative and washed with PBS three times. The exosome standard was then dehydrated in a series of increasing ethanol concentrations and analyzed with SEM with an accelerating voltage of 5 keV after gold sputtering.

## Results and discussion

Simulated LSPR spectra of gold nano-ellipsoids

To understand the properties of gold nano-ellipsoids, the transmission spectra and sensitivities of gold nano-ellipsoids with different sizes were simulated and measured. According to the Mie theory, the LSPR wavelength depends on the interparticle gap size and on the size of nanoparticles in air.[16] Larger particle sizes and shorter interparticle the gaps can lead to higher LSPR sensitivities.[23] Previous studies have reported that different nanoparticle center-to-center distance pitches nanoparticles have minor effects on the position of the LSPR peak.[36] Therefore, the nano-ellipsoids characteristics with different radii (r) and heights (h) (Fig. 3a–f) were simulated using the FDTD method. These calculations showed that the r and d values of the nano-ellipsoids are crucial parameters. Indeed, when r increases, the position of the peak is red-shifted, and its intensity increases significantly (Fig. 3a). For an $r$ = 25 nm, the spectra are too low to correctly determine the peak wavelength. The sensitivity of the gold nano-ellipsoids is increased with the increase of radius (Fig. 3b). The spectra of gold nano-ellipsoids were simulated at different heights when $r$ = 35 nm and $r$= 45 nm. Results showed that the values of h of the gold nano-ellipsoids substantially affected the peak position and intensity but ha d minor effects on the widths of the spectra (Fig. 3c and Fig. 3e). The results showed that increases of the gold nano-ellipsoids diameter resulted in a red shift of the peak and increased both the intensity and width of the LSPR spectra. Reducing the thickness of the gold nano-ellipsoids resulted in a red shift of the peak of the LSPR spectra, which became narrower and higher in intensity. These results are consistent with similar results in previous reports.[36,37] Thus, the heights of the gold nano-ellipsoids were chosen to be equal to 30 nm in the conducted experiment. The sensitivity of the gold nano-ellipsoids decreased when the height increasedf (Fig. 3d and Fig. 3f). When $h$ = 30 nm and $r$ = 35 nm, the sensitivity of the gold nano-ellipsoids was 173 nm/ refractive index unit (RIU), but when $h$ = 30 nm and $r$ = 45 nm, the sensitivity of the gold nano-ellipsoids was 240.9 nm/RIU. The sensitivities of the gold nano-ellipsoids with a radius of 45 nm are higher than those of nano-ellipsoids with a radius of 35 nm.

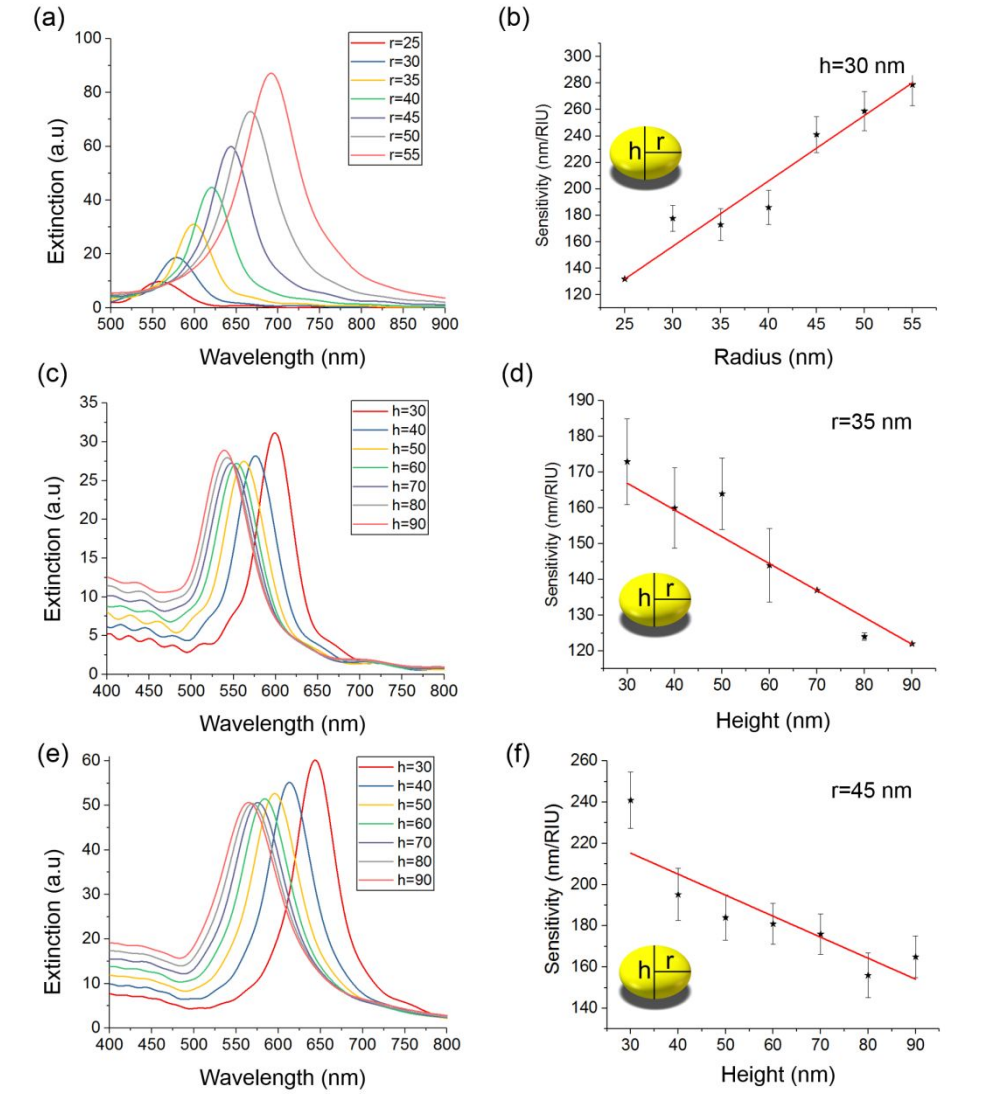


Figure 3. Simulated results of gold nano-ellipsoids with different structural parameters. (a) Extinction responses as a function of wavelength. The height of the gold nano-ellipsoids are set to 30 nm and their radii change from 25 to 55 nm. (b) Sensitivity cartogram of gold nano-ellipsoids with constant height and different radius. (c) Extinction responses as a function of wavelength. The radius is 35 nm and the height changes from 30 to 90 nm. (d) Sensitivity cartogram of gold nano-ellipsoids with a radius of 35 nm radius at different heights. (e) Extinction responses as a function of wavelength. The radius is set to 45 nm and the height changes from 30 to 90 nm. (f) Sensitivity cartogram of gold nano-ellipsoids with a radius of 45 nm and different heights.

To test the refractive index sensing capabilities of the nano-epllisoids, extinction spectra of the nano-epllisoids were also simulated for various solutions air, water, 1 M glucose, ethanol, and NaCl (5%, 10%, 15%, 20%, 25%)) with different refractive indices, and the outcomes are referred to the experiment results. The results show ed that increasing the refractive index of the sample resulted in a red shift of the extinction spectra. The structural parameters of the gold nano-ellipsoids were $h$ = 30 nm, $r$ = 35 nm and $r$ = 45 nm. When the radius was 45 nm, the position of the peak was red-shifted compared to the case at which the radius was 35 nm (Fig. 4a

and Fig. 4c). The sensitivity of the gold nano-ellipsoids with a 45 nm radius was higher than that of the 35 nm radius (Fig. 4b and Fig. 4d). The above results illustrate that the best LSPR responses should be obtained with gold nano-ellipsoids with $r$ = 45 nm and $h$ = 30 nm.

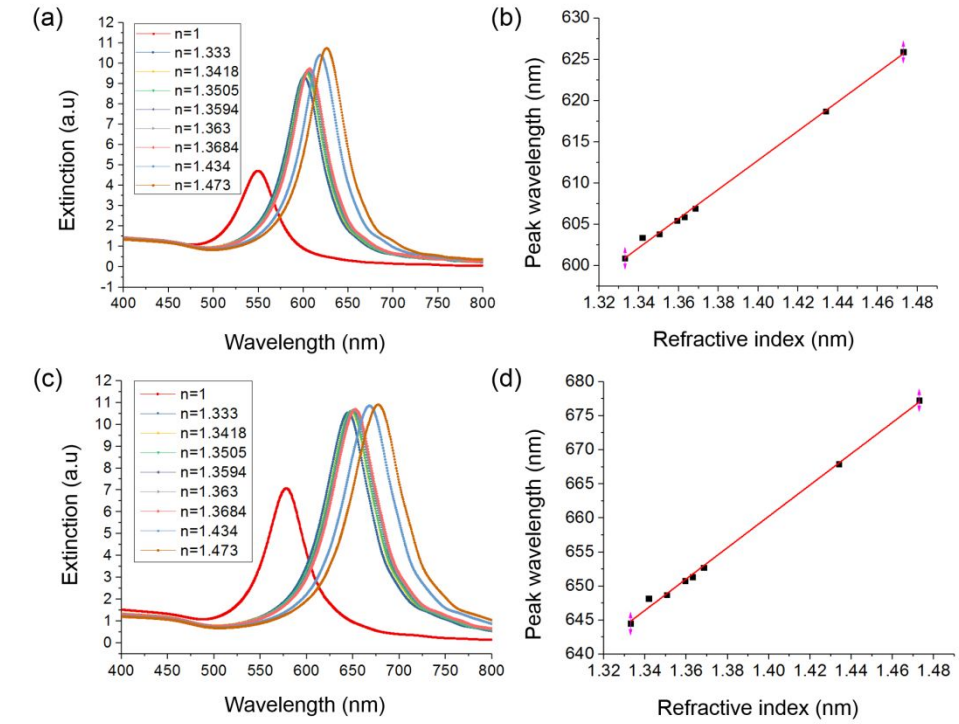


Figure 4. Extinction spectra of various solutions at different refractive indices. (a, b) Extinction responses as a function of wavelength and peak wavelength as a function of the refractive index for the case at which the radius is 35 nm and the height is 30 nm. (c, d) Extinction responses as a function of wavelength and peak wavelength as a function of the refractive index for the case at which the radius is 45 nm and the height is 30 nm.

## Characterization of the LSPR-based biosensor

The morphology of the prepared gold nano-ellipsoids was investigated by SEM. Fig. 5 displays the SEM image of gold nano-ellipsoid arrays on the substrate. The gold nanocylindricals had a larger in-plane size (Fig. 5a). However, each nanocylindrical shape pattern became nano-ellipsoidal after annealing owing to the surface tension (Fig. 5b). The arrangement of the gold nano-ellipsoids was the same as that of the AAO mask. The gold nano-ellipsoids had an average diameter of 90 nm. The size, density, and shape of the gold nano-ellipsoids depended on the characteristic of the AAO mask. By using AAO films with different pore sizes and thickness values, gold nano-epllisoids with different radii and heights could be synthesized. What calls for special attention is that the thickness of the Au film was recommended to be equal to 30 nm, otherwise the holes of the AAO mask would be easily blocked. A cross-sectional view of the arrays without the removal the AAO template is shown in Fig. 5c. This figure displays clearly the arrangement of gold nanoellipsiods and the excellent adhesion between the AAO mask and the substrate. The AFM characteristics of the gold nano-ellipsoids are shown in Fig. 5d. The SEM image shows highly ordered gold nanoellipsoid arrays with a large area in excess of 3000 $\mu m^2$ with no observable aggregation (Fig. 5e). By using this biosensor, nine different samples could be

detected simultaneously. During the fabrication of the biosensor, a nine-holes Al mould can be used repeatedly. Thus, it is easy to use this method to fabricate gold nano-ellipsoids using the AAO mask given that it is a low-cost, it is fast, and can be used for large-scale applications. Using this approach, the AAO film and the substrates, the AAO film was transferred onto the substrates following the simple hydrophilic treatment of an AAO film and the substrates. Subsequently, the nano-ellipsoid arrays were deposited on the substrates without any expensive and tedious process, such as electron beam evaporation, that constitutes a simple, inexpensive, and robust method for the fabrication of nanoparticle arrays.

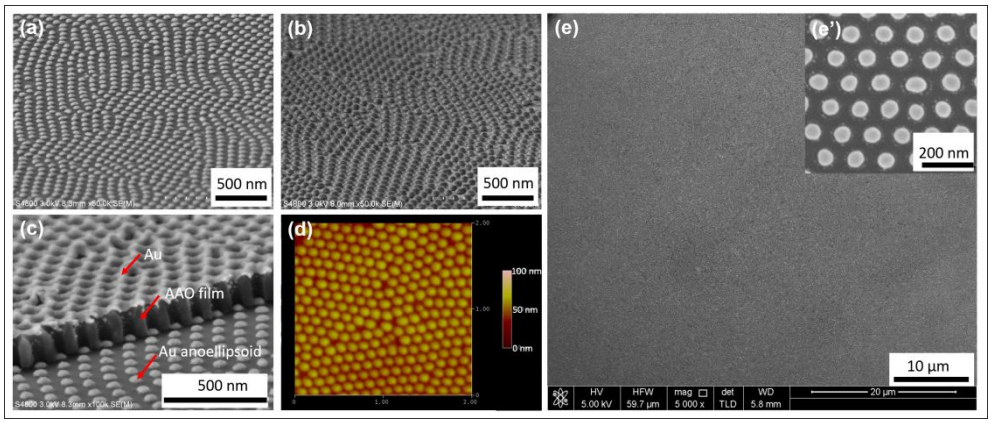


Figure 5. Scanning electron microscopy (SEM) and atomic force microscopy (AFM) images of gold nano-ellipsoid arrays with Au deposited with electron beam evaporation. (a) Before thermal annealing. (b) After thermal annealing. (c) A 45° side view of the gold nanoellipsiod and AAO film. (d) AFM images of the gold nano-ellipsoid arrays. (e) A large area of gold nanoellipsiods on the substrate. (e') is the partially enlarged view of (e).

## Functional test of the LSPR-based biosensor

To verify the sensitivity of the LSPR-based biosensor, we first tested the refractive index sensitivities of different solutions. The plasmonic performance of the prepared samples was measured with optical spectrophotometry by changing the medium above the nano-ellipsoids between different refractive index solutions. Fig. 6a shows the extinction spectra of the gold nano-epllisoids for different refractive indices for different solutions. Increasing the refractive index of the sample causes the extinction spectra to be red-shifted. The peak wavelength of the extinction spectra increases as a function of the increased refractive index. Additionally, the refractive index sensitivity of the LSPR-based biosensor is approximately 306 nm/RIU ((625.57-610.25)/(1.38-1.33)) (Fig. 6b). Results show that the biosensor has a good response as a function of therefractive index.

Functional tests wereLSPR-based biosensor carried out using the LSPR-based biosensor based on tests of the a) modification process of the anti-CD63 antibody and b) the reaction between the anti-CD63 antibody and exosomes. Exosomes detection utilized common exosome markers, such as tetraspanins (CD63, CD9, and CD81),[38–40] and the membrane transport and tumor-specific gene 101 (tsg101).[41] Among these markers, anti-CD63 has been extensively used for exosome capture owing to its expression on the exosome surfaces, and has been accepted as a

general exosome marker.[42] Exosomes can react with the anti-CD63 antibody in the biosensor and induces a shift of the LSPR wavelength of the underlying gold nano-ellipsoids. Fig. 6c illustrates that the combined reaction during the modification process can cause the extinction spectra to be red-shifted. Additionally, we utilized human immunoglobulin G (IgG) to demonstrate the specific capture and detection of CD63-positive exosomes. In a typical assay, human IgG was injected into the channel and the wavelength shift was recorded by the spectrometer. Fig. S2 shows that a few spectral shifts of the gold nano-ellipsoids as a function of the LSPR wavelength. The TEM image shows the sizes and morphologies of the exosomes before detection (Fig. 6c') and the SEM image shows exosomes after their detection and uniform capturing on the gold nano-ellipsoids (Fig. 6d). Overall, the sensing performance of our biosensor is highly comparable to the current state-of-the-art in reference to the LSPR platform.[21,23]

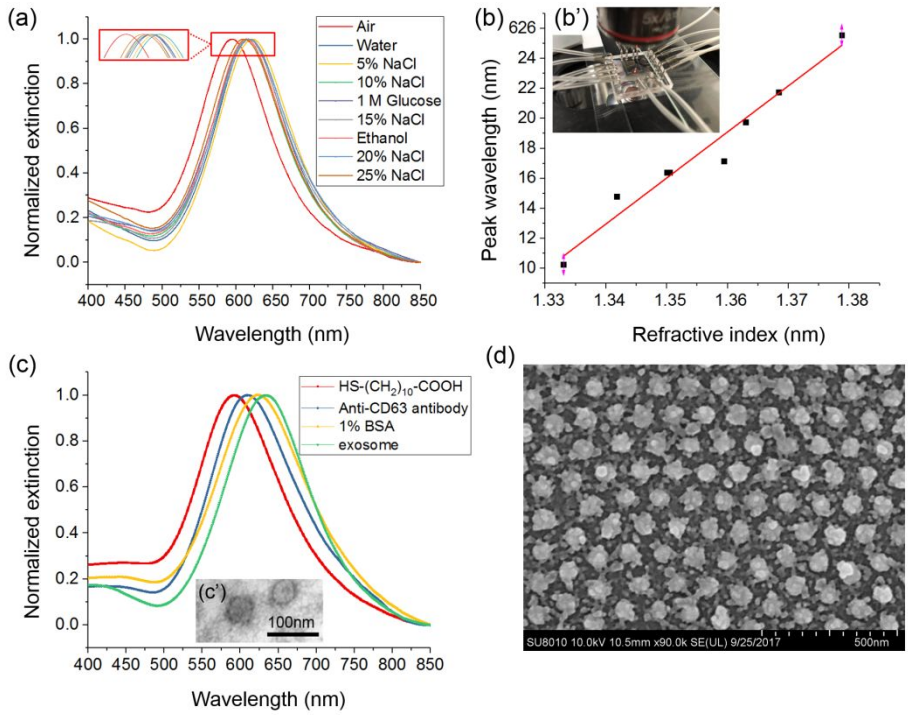


Figure 6. Testing results of the LSPR-based biosensor. (a) Normalized extinction spectra as a function of the refractive index for different solutions. (b) Peak wavelengths as a function of the refractive index for different solutions. (b') The biosensor with nine channels on the LSPR detection platform. (c) Normalized extinction spectral changes during the functionalized process. The inset image is a high-magnification transmission electron microscopy of exosomes before detection. (d) Scanning electron microscopy image of exosomes captured by the functionalized LSPR-based biosensor.

## Performance of the LSPR-based biosensor

To test the performance of the LSPR-based biosensor, different binding times between the anti-CD63 antibody and the exosomes and different exosome concentrations were detected using the LSPR-based biosensor. Figs. 7a and 7b show the extinction spectra and peak wavelength at

different binding times between the anti-CD63 antibody and exosomes. These results illustrats that the peak wavelength of the extinction spectra increases as the binding time increases. The binding process between the anti-CD63 antibody and exosomes has reached saturation at approximately 50 min (Fig. 7b). Fig. 8 shows the extinction spectra under at concentration of exosomes (1 ng/mL, 10 ng/mL, $1\times10^2$ ng/mL, $1\times10^3$ ng/mL, and $1\times10^3$ ng/mL). Results illustrate that the peak wavelength of the extinction spectra increases as the concentration of exosomes increases. After the capture of the exosomes, 1× PBS buffer solution at a volume of 1 mL was injected to rinse the biosensor channel and verify the capture of the exosomes on the gold nano-ellipsoids. The evoked responses of these five concentrations were utilized to test the ability to conduct exosome detection with the LSPR-based biosensor, as shown in Fig. 8. The limit of detection was analysed according to the reported study[43]. The peak wavelength of the exosomes was 620.98 nm when their concentration was 1 ng/mL. The peak wavelength of the anti-CD63 antibody was 619.44 at an exosome concentration of 1 ng/mL approximately. In addition, a wavelength shift of 1.54 nm is a weak response which is closed to the negative control for human IgG. The testing concentration limit of the exosomes was approximately 1 ng/mL. This indicated that the exosomes were immobilized onto the gold nano-ellipsoids and caused the extinction shift.

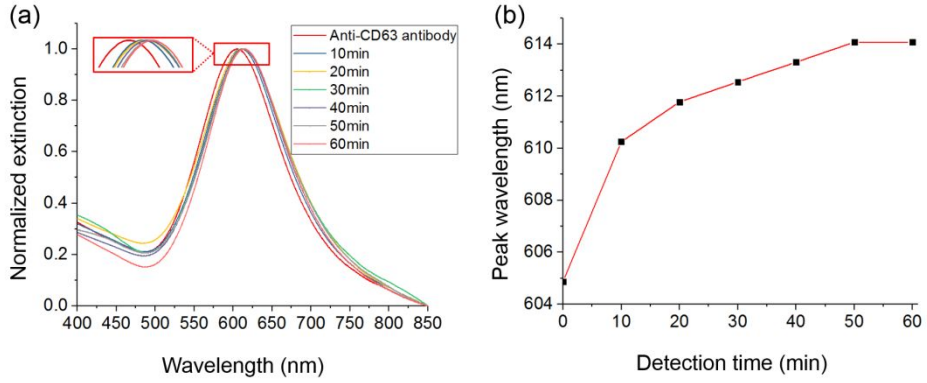


Figure 7. Performance of the LSPR-based biosensor at different binding time of the anti-CD63 antibody and exosomes. (a) Normalized extinction spectra as a function of the wavelength, and (b) peak wavelength response as a function of detection time.

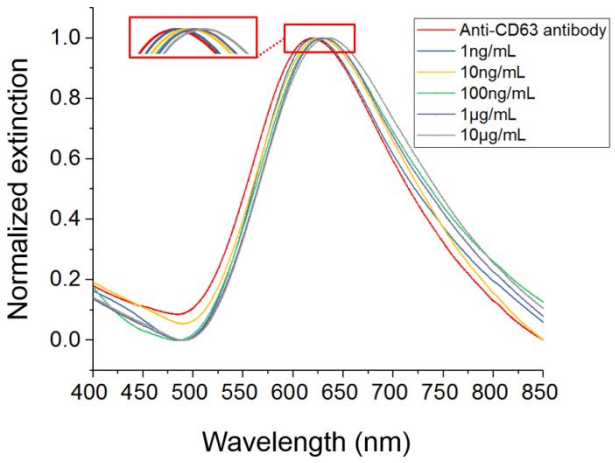


Figure 8. Performance of the LSPR-based biosensor at different exosome concentrations.

Targeted therapy of cancer is becoming increasingly popular. However, chemotherapy is still

the main treatment owing to the lack of an adequate number of specific targets.[44] Accordingly, the identification of the new noninvasive biomarkers for cancer is a key issue for cancer diagnosis and therapy.[45] Exosome detection hasled to increased attention in the field of biomedical and biological detection. Numerous studies have shown the potential use of circulating exosomes as novel biomarkers for monitoring and predicting a number of complex diseases, including cancer.[46] Unlike cells, for which the viability after isolation also needs to be considered, exosomes are known to be more actable against environmental change.[1,5,47] For this reason, the ribonucleic acid (RNA) contained in exosomes could be released using lysis buffers. Our proposed approach is an option to find new exosome biomarkers for cancer.

The LSPR-based biosensor is a platform technology with four key innovative aspects over the commonly used methods. (i) Fabrication of the nano-ellipsoids is easy, fast, and large-scale, based on the use of AAO films as the templates to for the evaporation of gold. The robust fabrication method of the biosensor saves consumables, and leads low device failure rates. (ii) Gold nano-ellipsoids prepared by this method are uniform and perform better than those prepared by evaporation and annealing. (iii) The biosensor detects exosomes using as little as 50 μL aliquots in < 4 h, whereas ELISA requires > 200 μL sample volumes and twice of time.[48] The ability to detect exosomes from small volumes is highly advantageous in the case where the sample is limited. (iv) Exosomes are allowed for downstream analyses after they are captured on the biosensor. In future experiments, we will expend efforts to study additional exosome characteristics using different types of bodily fluids (e.g., blood, cerebrospinal fluid, urine, ascitic fluids) in cooperation with biomedical laboratories.

## Conclusions

A simple, inexpensive, and robust LSPR-based biosensor was proposed to detect exosomes in buffer solutions. The fabrication method of the biosensor was optimized based on a simple annealing process and the use of an AAO film as a gold evaporation template. Overall, the method is low-cost, time-saving, and applicable to large areas. The gold nano-ellipsoid arrays fabricated with this method were ordered compared with simple annealing. The functionalization of the biosensor was easily achieved following the integration of the sensor with microfluidics. Exosomes could be uniformly absorbed on the surface of gold nano-ellipsoids after the functional modification of the anti-CD63 antibody on the biosensor. Different refractive index solutions were used to test the responses of the biosensor. In addition, exosome samples at five different concentrations were utilized to test the detection ability of the biosensor. A sensitive biosensor was built to successfully detect exosomes in buffer solutions with approximate concentrations of 1 ng/mL. In conclusion, this biosensor, which is simple to use and fabricate, has the ability to detect minute exosome concentration. In the future, this LSPR-based biosensor could provide a useful platform to facilitate clinical investigations of exosomes for non-invasive disease diagnoses.

## Acknowledgement

The project was supported by The National Key R. & D. Plan (2017YFB0405400), China

Postdoctoral Science Foundation (2018M641448), The National Natural Science Foundation of China (61774175 and 61674146), The Opened Fund of the State Key Laboratory of Integrated Optoelectronics (No. IOSKL2017KF12), The Key Program of Natural Science Foundation of Beijing (4181001), The leading project of youth academic team @ Minzu University of China (Sensor and microsystem: 317201929) and Research project of scientific research equipment of CAS (YJKYYQ20170043).

## Supporting Information

The LSPR detecting platform, Specificity test of the LSPR-based biosensor and Characterization of exosomes were concluded in the Supporting Information.

## Conflict of Interest Disclosure

The authors declare no competing financial interest.

## Reference

(1) Li, M.; Zeringer, E.; Barta, T.; Schageman, J.; Cheng, A.; Vlassov, A. V. Analysis of the RNA Content of the Exosomes Derived from Blood Serum and Urine and Its Potential as Biomarkers. *Philos. Trans. R. Soc. B Biol. Sci.* **2014**, *369* (1652), 20130502–20130502. https://doi.org/10.1098/rstb.2013.0502.

(2) Pocsfalvi, G.; Stanly, C.; Vilasi, A.; Fiume, I.; Capasso, G.; Turiák, L.; Buzas, E. I.; Vékey, K. Mass Spectrometry of Extracellular Vesicles: MASS SPECTROMETRY OF EXTRACELLULAR VESICLES. *Mass Spectrom. Rev.* **2016**, *35* (1), 3–21. https://doi.org/10.1002/mas.21457.

(3) Wei, M.; Yang, T.; Chen, X.; Wu, Y.; Deng, X.; He, W.; Yang, J.; Wang, Z. Malignant Ascites-Derived Exosomes Promote Proliferation and Induce Carcinoma-Associated Fibroblasts Transition in Peritoneal Mesothelial Cells. *Oncotarget* **2017**, *8* (26). https://doi.org/10.18632/oncotarget.15040.

(4) Yagi, Y.; Ohkubo, T.; Kawaji, H.; Machida, A.; Miyata, H.; Goda, S.; Roy, S.; Hayashizaki, Y.; Suzuki, H.; Yokota, T. Next-Generation Sequencing-Based Small RNA Profiling of Cerebrospinal Fluid Exosomes. *Neurosci. Lett.* **2017**, *636*, 48–57. https://doi.org/10.1016/j.neulet.2016.10.042.

(5) Sunkara, V.; Woo, H.-K.; Cho, Y.-K. Emerging Techniques in the Isolation and Characterization of Extracellular Vesicles and Their Roles in Cancer Diagnostics and Prognostics. *The Analyst* **2016**, *141* (2), 371–381. https://doi.org/10.1039/C5AN01775K.

(6) Liu, F.; Vermesh, O.; Mani, V.; Ge, T. J.; Madsen, S. J.; Sabour, A.; Hsu, E.-C.; Gowrishankar, G.; Kanada, M.; Jokerst, J. V.; et al. The Exosome Total Isolation Chip. *ACS Nano* **2017**, *11* (11), 10712–10723. https://doi.org/10.1021/acsnano.7b04878.

(7) Kang, Y.-T.; Kim, Y. J.; Bu, J.; Cho, Y.-H.; Han, S.-W.; Moon, B.-I. High-Purity Capture and Release of Circulating Exosomes Using an Exosome-Specific Dual-Patterned Immunofiltration (ExoDIF) Device. *Nanoscale* **2017**, *9* (36), 13495–13505. https://doi.org/10.1039/C7NR04557C.

(8) Reátegui, E.; van der Vos, K. E.; Lai, C. P.; Zeinali, M.; Atai, N. A.; Aldikacti, B.; Floyd,

F. P.; H. Khankhel, A.; Thapar, V.; Hochberg, F. H.; et al. Engineered Nanointerfaces for Microfluidic Isolation and Molecular Profiling of Tumor-Specific Extracellular Vesicles. *Nat. Commun.* **2018**, *9* (1). https://doi.org/10.1038/s41467-017-02261-1.

(9) Boriachek, K.; Islam, Md. N.; Gopalan, V.; Lam, A. K.; Nguyen, N.-T.; Shiddiky, M. J. A. Quantum Dot-Based Sensitive Detection of Disease Specific Exosome in Serum. *The Analyst* **2017**, *142* (12), 2211–2219. https://doi.org/10.1039/C7AN00672A.

(10) Zhang, P.; He, M.; Zeng, Y. Ultrasensitive Microfluidic Analysis of Circulating Exosomes Using a Nanostructured Graphene Oxide/Polydopamine Coating. *Lab. Chip* **2016**, *16* (16), 3033–3042. https://doi.org/10.1039/C6LC00279J.

(11) Vaidyanathan, R.; Naghibosadat, M.; Rauf, S.; Korbie, D.; Carrascosa, L. G.; Shiddiky, M. J. A.; Trau, M. Detecting Exosomes Specifically: A Multiplexed Device Based on Alternating Current Electrohydrodynamic Induced *Nanoshearing*. *Anal. Chem.* **2014**, *86* (22), 11125–11132. https://doi.org/10.1021/ac502082b.

(12) Chen, J.; Xu, Y.; Lu, Y.; Xing, W. Isolation and Visible Detection of Tumor-Derived Exosomes from Plasma. *Anal. Chem.* **2018**, *90* (24), 14207–14215. https://doi.org/10.1021/acs.analchem.8b03031.

(13) Gao, D.; Liu, H.; Jiang, Y.; Lin, J.-M.; Gao, D.; Liu, H.; Jiang, Y. Recent Developments in Microfluidic Devices for in Vitro Cell Culture for Cell-Biology Research. *TrAC Trends Anal. Chem.* **2012**, *35*, 150–164. https://doi.org/10.1016/j.trac.2012.02.008.

(14) Hisey, C. L.; Dorayappan, K. D. P.; Cohn, D. E.; Selvendiran, K.; Hansford, D. J. Microfluidic Affinity Separation Chip for Selective Capture and Release of Label-Free Ovarian Cancer Exosomes. *Lab. Chip* **2018**, *18* (20), 3144–3153. https://doi.org/10.1039/C8LC00834E.

(15) Sepúlveda, B.; Angelomé, P. C.; Lechuga, L. M.; Liz-Marzán, L. M. LSPR-Based Nanobiosensors. *Nano Today* **2009**, *4* (3), 244–251. https://doi.org/10.1016/j.nantod.2009.04.001.

(16) Geng, Z.; Kan, Q.; Yuan, J.; Chen, H. A Route to Low-Cost Nanoplasmonic Biosensor Integrated with Optofluidic-Portable Platform. *Sens. Actuators B Chem.* **2014**, *195*, 682–691. https://doi.org/10.1016/j.snb.2014.01.110.

(17) Jia, S.; Bian, C.; Sun, J.; Tong, J.; Xia, S. A Wavelength-Modulated Localized Surface Plasmon Resonance (LSPR) Optical Fiber Sensor for Sensitive Detection of Mercury(II) Ion by Gold Nanoparticles-DNA Conjugates. *Biosens. Bioelectron.* **2018**, *114*, 15–21. https://doi.org/10.1016/j.bios.2018.05.004.

(18) Kaye, S.; Zeng, Z.; Sanders, M.; Chittur, K.; Koelle, P. M.; Lindquist, R.; Manne, U.; Lin, Y.; Wei, J. Label-Free Detection of DNA Hybridization with a Compact LSPR-Based Fiber-Optic Sensor. *The Analyst* **2017**, *142* (11), 1974–1981. https://doi.org/10.1039/C7AN00249A.

(19) Li, N.; Lu, Y.; Li, S.; Zhang, Q.; Wu, J.; Jiang, J.; Liu, G. L.; Liu, Q. Monitoring the Electrochemical Responses of Neurotransmitters through Localized Surface Plasmon Resonance Using Nanohole Array. *Biosens. Bioelectron.* **2017**, *93*, 241–249. https://doi.org/10.1016/j.bios.2016.08.105.

(20) Li, S.; Liu, J.; Lu, Y.; Zhu, L.; Li, C.; Hu, L.; Li, J.; Jiang, J.; Low, S.; Liu, Q. Mutual Promotion of Electrochemical-Localized Surface Plasmon Resonance on Nanochip for Sensitive Sialic Acid Detection. *Biosens. Bioelectron.* **2018**, *117*, 32–39.

https://doi.org/10.1016/j.bios.2018.05.062.

(21) Thakur, A.; Qiu, G.; Ng, S.-P.; Guan, J.; Yue, J.; Lee, Y.; Wu, C.-M. L. Direct Detection of Two Different Tumor-Derived Extracellular Vesicles by SAM-AuNIs LSPR-based biosensor. *Biosens. Bioelectron.* **2017**, *94*, 400–407. https://doi.org/10.1016/j.bios.2017.03.036.

(22) Im, H.; Shao, H.; Park, Y. I.; Peterson, V. M.; Castro, C. M.; Weissleder, R.; Lee, H. Label-Free Detection and Molecular Profiling of Exosomes with a Nano-Plasmonic Sensor. *Nat. Biotechnol.* **2014**, *32* (5), 490–495. https://doi.org/10.1038/nbt.2886.

(23) Bonyár, A.; Csarnovics, I.; Veres, M.; Himics, L.; Csik, A.; Kámán, J.; Balázs, L.; Kökényesi, S. Investigation of the Performance of Thermally Generated Gold Nanoislands for LSPR and SERS Applications. *Sens. Actuators B Chem.* **2018**, *255*, 433–439. https://doi.org/10.1016/j.snb.2017.08.063.

(24) Jain, P. K.; El-Sayed, M. A. Plasmonic Coupling in Noble Metal Nanostructures. *Chem. Phys. Lett.* **2010**, *487* (4–6), 153–164. https://doi.org/10.1016/j.cplett.2010.01.062.

(25) Wu, T.; Lin, Y.-W. Surface-Enhanced Raman Scattering Active Gold Nanoparticle/Nanohole Arrays Fabricated through Electron Beam Lithography. *Appl. Surf. Sci.* **2018**, *435*, 1143–1149. https://doi.org/10.1016/j.apsusc.2017.11.213.

(26) Liu, J.; Zhang, S.; Ma, Y.; Shao, J.; Lu, B.; Chen, Y. Gold Nanopillar Arrays as Biosensors Fabricated by Electron Beam Lithography Combined with Electroplating. *Appl. Opt.* **2015**, *54* (9), 2537. https://doi.org/10.1364/AO.54.002537.

(27) Couture, M.; Brulé, T.; Laing, S.; Cui, W.; Sarkar, M.; Charron, B.; Faulds, K.; Peng, W.; Canva, M.; Masson, J.-F. High Figure of Merit (FOM) of Bragg Modes in Au-Coated Nanodisk Arrays for Plasmonic Sensing. *Small* **2017**, *13* (38), 1700908. https://doi.org/10.1002/smll.201700908.

(28) Lin, D.-Z.; Chuang, P.-C.; Liao, P.-C.; Chen, J.-P.; Chen, Y.-F. Increasing the Spectral Shifts in LSPR Biosensing Using DNA-Functionalized Gold Nanorods in a Competitive Assay Format for the Detection of Interferon-γ. *Biosens. Bioelectron.* **2016**, *81*, 221–228. https://doi.org/10.1016/j.bios.2016.02.071.

(29) Klinghammer, S.; Uhlig, T.; Patrovsky, F.; Böhm, M.; Schütt, J.; Pütz, N.; Baraban, L.; Eng, L. M.; Cuniberti, G. Plasmonic Biosensor Based on Vertical Arrays of Gold Nanoantennas. *ACS Sens.* **2018**, *3* (7), 1392–1400. https://doi.org/10.1021/acssensors.8b00315.

(30) Wang, C.; Wang, G.; Yang, R.; Sun, X.; Ma, H.; Sun, S. Hydrophilicity Reinforced Adhesion of Anodic Alumina Oxide Template Films to Conducting Substrates for Facile Fabrication of Highly Ordered Nanorod Arrays. *Langmuir* **2017**, *33* (2), 503–509. https://doi.org/10.1021/acs.langmuir.6b03999.

(31) Al-Haddad, A.; Zhan, Z.; Wang, C.; Tarish, S.; Vellacheria, R.; Lei, Y. Facile Transferring of Wafer-Scale Ultrathin Alumina Membranes onto Substrates for Nanostructure Patterning. *ACS Nano* **2015**, *9* (8), 8584–8591. https://doi.org/10.1021/acsnano.5b03789.

(32) Masuda, H.; Yasui, K.; Nishio, K. Fabrication of Ordered Arrays of Multiple Nanodots Using Anodic Porous Alumina as an Evaporation Mask. *Adv. Mater.* **2000**, *12* (14), 1031–1033. https://doi.org/10.1002/1521-4095(200007)12:14<1031::AID-ADMA1031>3.0.CO;2-R.

(33) Wen, L.; Xu, R.; Mi, Y.; Lei, Y. Multiple Nanostructures Based on Anodized Aluminium

Oxide Templates. *Nat. Nanotechnol.* **2017**, *12* (3), 244–250. https://doi.org/10.1038/nnano.2016.257.

(34) Zhao, C.; Chen, A.; Ji, X.; Zhu, Y.; Gui, X.; Huang, F.; Tang, Z. Growth of Vertically Aligned ZnO Nanowire Arrays on ZnO Single Crystals. *Mater. Lett.* **2015**, *154*, 40–43. https://doi.org/10.1016/j.matlet.2015.04.053.

(35) Chen, P.; Chung, M. T.; McHugh, W.; Nidetz, R.; Li, Y.; Fu, J.; Cornell, T. T.; Shanley, T. P.; Kurabayashi, K. Multiplex Serum Cytokine Immunoassay Using Nanoplasmonic Biosensor Microarrays. *ACS Nano* **2015**, *9* (4), 4173–4181. https://doi.org/10.1021/acsnano.5b00396.

(36) Demirdjian, B.; Bedu, F.; Ranguis, A.; Ozerov, I.; Henry, C. R. Water Adsorption by a Sensitive Calibrated Gold Plasmonic Nanosensor. *Langmuir* **2018**, *34* (19), 5381–5385. https://doi.org/10.1021/acs.langmuir.8b00040.

(37) Chen, S.; Svedendahl, M.; Käll, M.; Gunnarsson, L.; Dmitriev, A. Ultrahigh Sensitivity Made Simple: Nanoplasmonic Label-Free Biosensing with an Extremely Low Limit-of-Detection for Bacterial and Cancer Diagnostics. *Nanotechnology* **2009**, *20* (43), 434015. https://doi.org/10.1088/0957-4484/20/43/434015.

(38) He, M.; Crow, J.; Roth, M.; Zeng, Y.; Godwin, A. K. Integrated Immunoisolation and Protein Analysis of Circulating Exosomes Using Microfluidic Technology. *Lab. Chip* **2014**, *14* (19), 3773. https://doi.org/10.1039/C4LC00662C.

(39) Jørgensen, M.; Bæk, R.; Pedersen, S.; Søndergaard, E. K. L.; Kristensen, S. R.; Varming, K. Extracellular Vesicle (EV) Array: Microarray Capturing of Exosomes and Other Extracellular Vesicles for Multiplexed Phenotyping. *J. Extracell. Vesicles* **2013**, *2* (1), 20920. https://doi.org/10.3402/jev.v2i0.20920.

(40) Rupert, D. L. M.; Lässer, C.; Eldh, M.; Block, S.; Zhdanov, V. P.; Lotvall, J. O.; Bally, M.; Höök, F. Determination of Exosome Concentration in Solution Using Surface Plasmon Resonance Spectroscopy. *Anal. Chem.* **2014**, *86* (12), 5929–5936. https://doi.org/10.1021/ac500931f.

(41) Willms, E.; Johansson, H. J.; Mäger, I.; Lee, Y.; Blomberg, K. E. M.; Sadik, M.; Alaarg, A.; Smith, C. I. E.; Lehtiö, J.; EL Andaloussi, S.; et al. Cells Release Subpopulations of Exosomes with Distinct Molecular and Biological Properties. *Sci. Rep.* **2016**, *6* (1). https://doi.org/10.1038/srep22519.

(42) Chiu, Y.-J.; Cai, W.; Shih, Y.-R. V.; Lian, I.; Lo, Y.-H. A Single-Cell Assay for Time Lapse Studies of Exosome Secretion and Cell Behaviors. *Small* **2016**, *12* (27), 3658–3666. https://doi.org/10.1002/smll.201600725.

(43) Qiu, G.; Thakur, A.; Xu, C.; Ng, S.-P.; Lee, Y.; Wu, C.-M. L. Detection of Glioma-Derived Exosomes with the Biotinylated Antibody-Functionalized Titanium Nitride Plasmonic Biosensor. *Adv. Funct. Mater.* **2019**, *29* (9), 1806761. https://doi.org/10.1002/adfm.201806761.

(44) Halvaei, S.; Daryani, S.; Eslami-S, Z.; Samadi, T.; Jafarbeik-Iravani, N.; Bakhshayesh, T. O.; Majidzadeh-A, K.; Esmaeili, R. Exosomes in Cancer Liquid Biopsy: A Focus on Breast Cancer. *Mol. Ther. - Nucleic Acids* **2018**, *10*, 131–141. https://doi.org/10.1016/j.omtn.2017.11.014.

(45) Cazzoli, R.; Buttitta, F.; Di Nicola, M.; Malatesta, S.; Marchetti, A.; Rom, W. N.; Pass, H. I. MicroRNAs Derived from Circulating Exosomes as Noninvasive Biomarkers for

Screening and Diagnosing Lung Cancer. *J. Thorac. Oncol.* **2013**, *8* (9), 1156–1162. https://doi.org/10.1097/JTO.0b013e318299ac32.

(46) Xia, Y.; Liu, M.; Wang, L.; Yan, A.; He, W.; Chen, M.; Lan, J.; Xu, J.; Guan, L.; Chen, J. A Visible and Colorimetric Aptasensor Based on DNA-Capped Single-Walled Carbon Nanotubes for Detection of Exosomes. *Biosens. Bioelectron.* **2017**, *92*, 8–15. https://doi.org/10.1016/j.bios.2017.01.063.

(47) Sokolova, V.; Ludwig, A.-K.; Hornung, S.; Rotan, O.; Horn, P. A.; Epple, M.; Giebel, B. Characterisation of Exosomes Derived from Human Cells by Nanoparticle Tracking Analysis and Scanning Electron Microscopy. *Colloids Surf. B Biointerfaces* **2011**, *87* (1), 146–150. https://doi.org/10.1016/j.colsurfb.2011.05.013.

(48) Duan, L.; Wang, Y.; Li, S. S.; Wan, Z.; Zhai, J. Rapid and Simultaneous Detection of Human Hepatitis B Virus and Hepatitis C Virus Antibodies Based on a Protein Chip Assay Using Nano-Gold Immunological Amplification and Silver Staining Method. *BMC Infect. Dis.* **2005**, *5* (1). https://doi.org/10.1186/1471-2334-5-53.

**Table of Contents Graphic**